*remote sensing*

MDPI

*Article*

# Recent Changes in Groundwater and Surface Water in Large Pan-Arctic River Basins

**Hong Lin [1], Xiao Cheng [1,2,*], Lei Zheng [1,2], Xiaoqing Peng [3], Wei Feng [1] and Fukai Peng [1,2]**

[1] School of Geospatial Engineering and Science, Sun Yat-sen University, Zhuhai 519000, China; linh48@mail2.sysu.edu.cn (H.L.); zhenglei6@mail.sysu.edu.cn (L.Z.); fengwei@mail.sysu.edu.cn (W.F.); pengfk@mail.sysu.edu.cn (F.P.)
[2] Southern Marine Science and Engineering Guangdong Laboratory (Zhuhai), Zhuhai 519082, China
[3] Key Laboratory of Western China's Environmental Systems (Ministry of Education), College of Earth and Environmental Sciences, Lanzhou University, Lanzhou 730000, China; pengxq13@lzu.edu.cn
* Correspondence: chengxiao9@mail.sysu.edu.cn

**Abstract:** Surface and groundwater in large pan-Arctic river basins are changing rapidly. High-quality estimates of these changes are challenging because of the limits on the data quality and time span of satellite observations. Here, the term pan-Arctic river refers to the rivers flowing to the Arctic Ocean basin. In this study, we provide a new evaluation of groundwater storage (GWS) changes in the Lena, Ob, Yenisei, Mackenzie and Yukon River basins from the GRACE total water storage anomaly product, in situ runoff, soil moisture form models and a snow water equivalent product that has been significantly improved. Seasonal Trend decomposition using Loess was utilized to obtain trends in GWS. Changes in surface water (SW) between 1984 and 2019 in these basins were also examined based on the Joint Research Centre Global Surface Water Transition data. Results suggested that there were great GWS losses in the North American river basins, totaling approximately −219 km$^3$, and GWS gains in the Siberian river basins, totaling ~340 km$^3$, during 2002–2017. New seasonal and permanent SWs are the primary contributors to the SW transition, accounting for more than 50% of the area of the changed SW in each basin. Changes in the Arctic hydrological system will be more significant and various in the case of rapid and continuous changes in permafrost.

**Keywords:** Arctic; groundwater storage; surface water; GRACE; gravity; remote sensing

check for updates

**Citation:** Lin, H.; Cheng, X.; Zheng, L.; Peng, X.; Feng, W.; Peng, F. Recent Changes in Groundwater and Surface Water in Large Pan-Arctic River Basins. *Remote Sens.* **2022**, *14*, 607. https://doi.org/10.3390/rs14030607

Academic Editor: Simon Stisen

Received: 14 December 2021
Accepted: 25 January 2022
Published: 27 January 2022

**Publisher's Note:** MDPI stays neutral with regard to jurisdictional claims in published maps and institutional affiliations.

**Copyright:** © 2022 by the authors. Licensee MDPI, Basel, Switzerland. This article is an open access article distributed under the terms and conditions of the Creative Commons Attribution (CC BY) license (https://creativecommons.org/licenses/by/4.0/).

## 1. Introduction

Surface water and groundwater are changing rapidly because of significant climate warming in the Arctic region [1–5]. The increasing rate of temperature in the Arctic region is twice that of the global average [6,7]. Arctic amplification has intensified the melting of snow cover and glaciers, as well as widespread permafrost degradation [8–10]. In the cryosphere, permafrost degradation affects the hydrology [11] and increases the probability of natural disasters in high-altitude zones [12]. Permafrost, as the largest component in the cryosphere, is defined as a layer formed of soil and rock that remains below 0 °C for at least two consecutive years [13]. In this study, the term pan-Arctic river basin refers to the river basins of the Arctic Ocean. The five large river basins of the Arctic Ocean (Figure 1: Lena, Yenisei, Ob, Mackenzie, and Yukon) are largely covered by permafrost [14]. The hydrology in these basins exhibits strong responses to permafrost degradation. Large pan-Arctic river basins are considered representative of the cooling mechanism of the Earth's engine [11]. A better understanding of hydrological fluxes and storage at the large watershed scale is urgently required.

Permafrost warming has thickened the active layer and caused the development of talik (unfrozen ground beneath the water body) and thermokarst [15]. Deepening of the active layer may increase the drainage of water and increase runoff [16]. Open talik fully

penetrates an otherwise more extensive permafrost layer and connects surface water (SW) and groundwater [17]. Groundwater discharge to rivers increases in a warmer climate under the assumption of sufficient groundwater replenishment. Otherwise, the water table in the recharge portion of the river basins declines [18]. In the future, there will be a shift from surface water to groundwater-dominated systems in the Arctic, having notable impacts on the hydrological cycle [19].

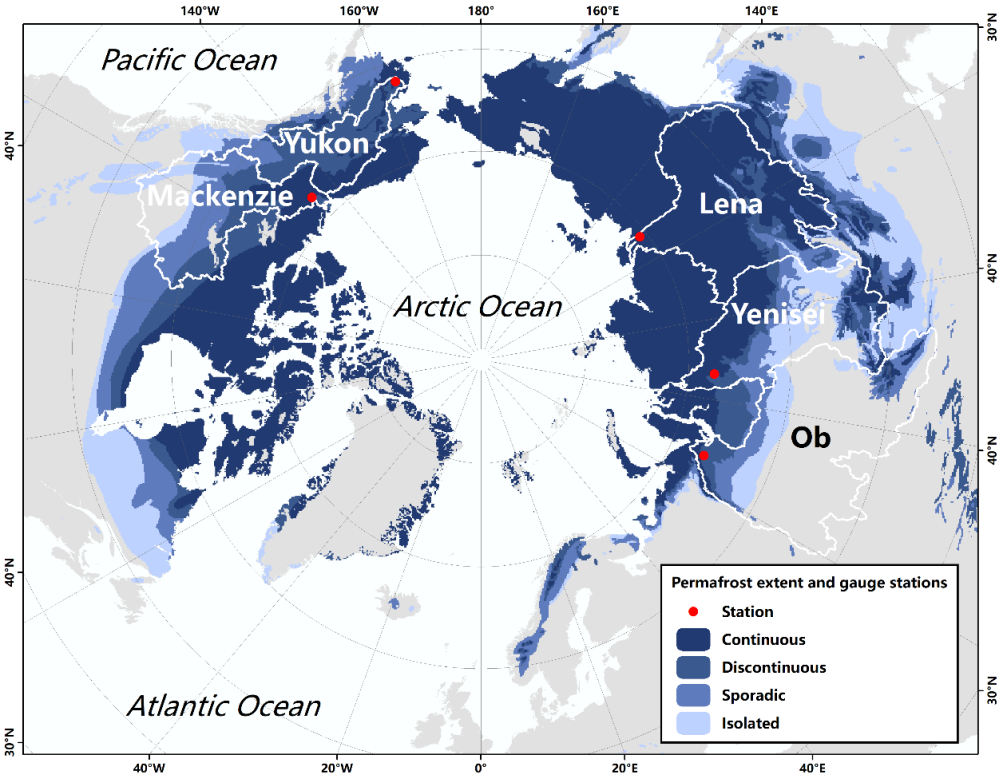



**Figure 1.** Locations of the five large pan-Arctic river basins: Lena, Yenisei, Ob, Mackenzie, and Yukon (https://worldmap.harvard.edu/data/geonode:wribasin_1eu, accessed on 1 March 2021); distribution of permafrost (https://nsidc.org/data/GGD318/versions/2, accessed on 13 April 2021) [20]; and locations of gauge stations.

Changes in Arctic rivers and lakes greatly contribute to surface water dynamics. The annual discharge of some Arctic rivers has prominently increased in recent decades from snow melting and permafrost thawing [21–25]. The increasing discharge results in dramatic impacts on the surface water transition and freshwater circulation in Arctic river basins. These impacts will be amplified in the future [26]. Remarkably, changes in Arctic rivers, in turn, can cause localized permafrost thaw [2,27,28], allowing greater connection between deep groundwater and surface water pathways [29,30]. Both the number and area of Artic lakes decreased significantly during 1973–1998 [31] and 1948–2013 in the Yukon basin, which was related to the warmer climate and permafrost degradation [32]. An increasing trend in thermokarst lakes in Siberia was detected during 1999–2018, which was related to climate warming and increased precipitation [33].

Groundwater is a crucial component of the hydrological cycle, affecting Arctic freshwater, ecosystems, and oceans [17,34–36]. In high-latitude regions, evaluating groundwater flux and storage is challenging because of limited hydrogeological data and seasonal changes in aquifer permeability [37,38]. Groundwater discharge is a source of freshwater, dissolved organic matter [39], pollutants [40–42], and greenhouse gases [43,44] to Arctic coastal waters. In recent decades, groundwater discharge has increased in the Yukon basin [45] and is expected to be enhanced because of the more frequent groundwater–surface water interactions [46].

Remote sensing is an effective technique to monitor surface water and groundwater dynamics. Data sets of surface water location, extent, and seasonality have been produced from satellite imagery [47–51]. Radar and optical systems serve as an important proxy for estimating high-resolution hydrological parameters [52–54]. At a large scale, the Gravity Recovery and Climate Experiment (GRACE) satellites have been widely used to monitor groundwater storage (GWS) changes in individual aquifers [55–62] and around the world [63–67].

Dramatic changes have been observed in the Arctic in recent years, and more timely and accurate evaluation of surface and groundwater is urgently required. As remote sensing algorithms and data quality are constantly improving, remote sensing products with higher accuracy are available for surface and groundwater dynamics analyses. Neglecting soil moisture in the calculation of GWS would be remiss as the Arctic is becoming more humid. A time series decomposition method is needed to obtain the trends in water storage components because the trends obtained from a simple trend analysis method can be mixed with seasonal signals and errors. Seasonal Trend decomposition using Loess (STL) was utilized to obtain trends in GWS. Loess is a smoother that can smooth y based on any given x along the scale of the independent variable [68]. The objectives of this study are as follows:

1. To present a new evaluation of the surface and groundwater dynamics in large pan-Arctic river basins during the longest satellite record period;
2. To examine the recent changes in groundwater and surface water over the Arctic based on a Seasonal Trend decomposition methodology.

In this study, the total water storage anomaly (TWSA) from GRACE, soil moisture (SM) from the Global Land Data Assimilation System (GLDAS) and Famine Early Warning Systems Network Land Data Assimilation System (FLDAS), snow water equivalent (SWE) from spaceborne radiometers and in situ runoff were used to evaluate GWS changes in 2002–2017. Joint Research Centre (JRC) Global Surface Water data were also used to evaluate the surface water transition by calculating the proportion in each area of the transition types over the period 1984–2019.

## 2. Data

### *2.1. GRACE Total Water Storage Anomalies Data Set*

The total water storage (TWS) changes in GRACE are represented as total water storage anomalies. The monthly gravitational anomaly data from April 2002 to January 2017 (https://podaac.jpl.nasa.gov/dataset/TELLUS_LAND_NC_RL05, accessed on 13 April 2021) were provided by GRACE Tellus Monthly Mass Grids [69–71]. Here, the gravitational anomaly refers to the gravitational change relative to the long-term mean. The resolution of the data is 1 arc-degree. The data in this data set are units of equivalent water thickness (EWT) that represent the changes in mass in terms of the vertical extent of water in centimeters. EWT has been widely used in previous studies of GWS changes [55,56,62]. EWT represents the changes in water depth per unit area and is conducive to the comparison of GWS changes in the five basins. In this study, the monthly surface mass change data were based on the RL 05 spherical harmonics from three centers: the Center for Space Research (CSR), GeoForschungsZentrum (GFZ) and Jet Propulsion Laboratory (JPL). Since the coefficients were independently produced by each center and the results are slightly different, the mean of the data sets from the three centers was used in this study.

### *2.2. Soil Moisture and Rainfall from Global Models*

Soil moisture data in the top 2 m of the soil profile were obtained from GLDAS-2.1 (https://hydro1.gesdisc.eosdis.nasa.gov/data/GLDAS/GLDAS_NOAH025_3H.2.1/, accessed on 21 September 2021) [72] and FLDAS (https://hydro1.gesdisc.eosdis.nasa.gov/data/FLDA S/FLDAS_NOAH01_C_GL_M.001/, accessed on 21 September 2021) [73]. The GLDAS-2.1 provided a 3-hourly 0.25° SM product, which was simulated with the Noah Model 3.6 in Land Information System Version 7. FLDAS provided a monthly 0.1° SM

product, simulated with the Noah 3.6.1 model. The mean value of the two SM products was used in this study. GLDAS-2.1 also provided the 3-hourly rainfall rate product. The annual rainfall anomalies in the five basins were calculated based on the rainfall rate product.

### 2.3. Snow Water Equivalent

The Northern Hemisphere terrestrial snow water equivalent data set (https://www.globsnow.info/swe/archive_v3.0/, accessed on 10 February 2021) [74] was provided by the European Space Agency. This data set is from 1980 to 2018 and mapped to 25 km Equal-Area Scalable Earth Grids (EASE Grids). The SWE Version 3 data set was derived from satellite-based passive microwave radiometer data (Nimbus-7 SMMR, DMSP SSM/I and SSMIS) and ground-based synoptic snow depth observations using Bayesian data assimilation, incorporating the HUT snow emission model [75,76]. Assimilation approaches for SWE retrieval were applied to the data, effectively improving the accuracy [77,78]. Moreover, after applying the bias correction method, the uncertainty of SWE Version 3 was significantly less than that of the previous versions [79].

### 2.4. Runoff

The runoff (surface water discharge) data measured at the most downstream gauge stations in the five large river basins (Figure 1) were provided by the Arctic Great Rivers Observatory (ArcticGRO) (https://arcticgreatrivers.org/discharge/, accessed on 15 March 2021) [80]. Daily discharges from ArcticGRO at Kyusyur in Lena, Igarka in Yenisei, Salekhard in Ob, the Arctic Red River in Mackenzie, and Pilot Station in Yukon were used in this study. The monthly runoff time series from April 2002 to January 2017 was calculated by summing the daily runoff.

### 2.5. Global Surface Water Transition

High-resolution (30 m) global surface water dynamics data were provided by the Joint Research Centre [51]. The surface water dynamics time series was updated to a longer period from 1984 to 2019 (http://global-surface-water.appspot.com/, accessed on 31 March 2021). Landsat 5, 7, and 8 images were used to generate these data. In the transition data, global surface water dynamics were categorized into 10 different cases: permanent, seasonal, new permanent, new seasonal, lost permanent, lost seasonal, seasonal to permanent, permanent to seasonal, ephemeral permanent, and ephemeral seasonal.

## 3. Methods

### 3.1. Framework

The flow path and major components of this study are shown in Figure 2. The basin boundaries of Lena, Yenisei, Ob, Mackenzie, and Yukon obtained from WorldMap (https://worldmap.harvard.edu/data/geonode:wribasin_1eu, accessed on 1 March 2021) were used to extract the TWSA, SM, SWE, and JRC transition data. For groundwater dynamics analysis, SM, SWE, and runoff data from April 2002 to January 2017 were used in this analysis since this period was coincident with the provided TWSA time series. Missing records in the TWSA and SWE time series were imputed using linear interpolation. Monthly soil moisture storage anomaly (SMSA), snow water storage anomaly (SnWSA), and runoff anomaly (RA) were calculated based on SM, SWE, and runoff time series, respectively.

Here, surface water storage anomaly (SWSA) was estimated from in situ RA in river basins. Groundwater storage anomalies (GWSAs) in the five basins were obtained by subtracting SMSA, SnWSA, and SWSA from TWSA. Then, the trends in GWSA in 2002–2017 were obtained using STL. For the surface water body dynamics analysis, surface water bodies were categorized into the changed SW type and unchanged SW type. The changed SW type refers to the surface water bodies that changed into another type or disappeared or emerged during the observation period. The unchanged SW type refers to the surface water bodies that remain unchanged. The changed SW type includes new permanent, new seasonal, lost permanent, lost seasonal, permanent to seasonal, and seasonal to perma-

nent SW. Unchanged SW types include permanent, seasonal, ephemeral permanent, and ephemeral seasonal SW.

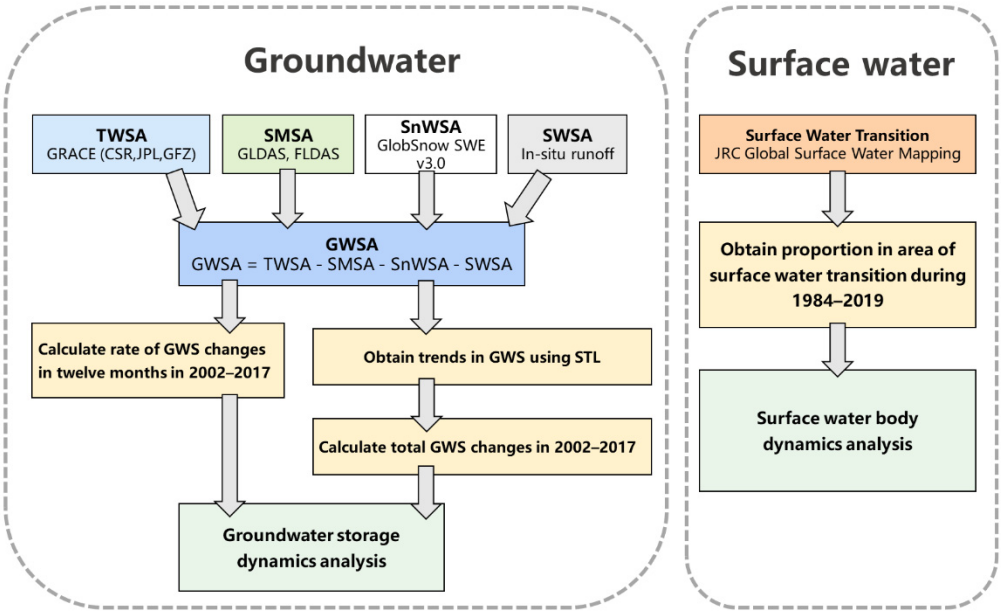



**Figure 2.** Framework of this study. The SA-ending refers to storage anomalies and snW is snow water.

### *3.2. Derivation of Groundwater Storage Anomaly*

TWS is controlled by different water storage components, including lake storage, runoff, ice and snow water storage, soil and vegetation moisture, and groundwater storage. The relationship of these water storage components can be presented in the following forms:

$$\mathrm{TWSA} = \mathrm{SMSA} + \mathrm{SnWSA} + \mathrm{SWSA} + \mathrm{GWSA} \quad (1)$$

where TWSA is the total water storage anomaly derived from GRACE, SMSA is the soil moisture storage anomaly derived from GLDAS and FLDAS, SnWSA is the snow water storage anomaly derived from SWE Version 3 product, SWSA is the surface water storage anomaly estimated from in situ runoff, and GWSA is the groundwater storage anomaly. To obtain GWS changes, Equation (1) can be collated as

$$\mathrm{GWSA} = \mathrm{TWSA} - \mathrm{SMSA} - \mathrm{SnWSA} - \mathrm{SWSA}. \quad (2)$$

Monthly uncertainty in GWSA was calculated as the square root of the sum of the monthly squared errors in TWSA, SMSA, and SnWSA. Rates of GWS changes were estimated by applying a least-squares fit. Uncertainty in trends in GWSA was derived from monthly uncertainty in GWSA based on the error propagation equation [81]. For TWSA derived from GRACE, the uncertainty was taken as the standard deviation of the TWS time series from the three centers (CSR, JPL, and GFZ). The uncertainty in SMSA was obtained from the standard deviation of SM from FLDAS and GLDAS. The uncertainty in SWE Version 3 was based on the overall root mean square error (RMSE) of 46.2 mm [79]. In situ runoff data were considered as true values and were absent in deriving uncertainty in GWSA.

In our study, we evaluated GWS dynamics at two different time scales. First, we estimated the trends in GWSA in different months from 2002 to 2017. Second, we estimated the volume changes of GWS in each basin over 15 years. We used STL to disaggregate the complete time series into three components: trend, seasonal, and remainder. Based on the trend components, we calculated the rates of GWS changes in the five basins. These rates were then used to derive the volume changes of GWS.

### *3.3. STL Time Series Decomposition*

Employing the Seasonal Trend decomposition using Loess (STL), a time series can be decomposed into three components: trend, seasonal, and remainder [68]:

$$D_{raw} = D_{trend} + D_{seasonal} + D_{remainder} \quad (3)$$

where $D_{raw}$ is the raw data, $D_{trend}$ is the trend in the data, $D_{seasonal}$ is the seasonal variation in the data, and $D_{remainder}$ is the remaining variation in the data.

In this study, we removed the variabilities with frequencies of $\leq$13 months from the GWSA time series to obtain the trends.

## 4. Results

### *4.1. Trends in Water Storage Components in 2002–2017*

The TWSA, SMSA, SnWSA, and RA time series in the five basins are shown in Figure S1. The trends in these water storage components and annual rainfall anomalies in 2002–2017 are shown in Figure 3. These trends were obtained using STL. There were almost no trends in RA in the five basins over the past 15 years (2002–2017). In Lena (Figure 3a), TWS decreased significantly in 2002–2013. SM and rainfall both decreased significantly during this period while the trend in SnWSA was slightly negative. In Yenisei and Ob (Figure 3b,c), TWS decreased significantly in 2002–2003 and 2012–2013. Subsequently, TWS increased in these two basins. Trends in TWSA in Mackenzie and Yukon (Figure 3d,e) were negative over 15 years. However, trends in SnWSA, SMSA, and RA were relatively slight in the two basins. Rain precipitation increased from 2016 to 2017 in Mackenzie and Yukon. TWS in Mackenzie increased in response to increased rainfall. However, TWS in Yukon continued to decrease during this period.

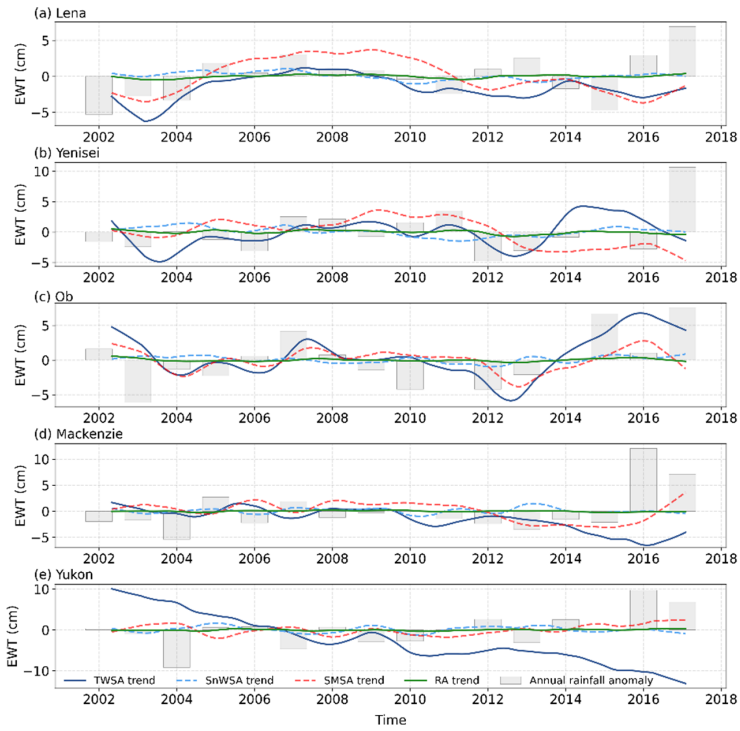



**Figure 3.** Trends in TWSA (deep blue line), SMSA (red dashed line), SnWSA (light blue dashed line), RA (green line), and annual rainfall anomaly (gray bar) from April 2002 to January 2017 in Lena, Yenisei, Ob, Mackenzie, and Yukon. EWT refers to equivalent water thickness.

### *4.2. Trends in Groundwater Storage Anomalies in Different Months*

Figure 4 illustrates the trends in GWSA in different months in 2002–2017. In Lena, GWSA trends were slightly negative ($-0.07 \pm 0.01$ cm/year) in May while GWSA trends

were positive during the other months, ranging from 0.17 ± 0.01 to 0.34 ± 0.01 cm/year. GWS increased more significantly in Yenisei than in Lena and Ob, where the highest rate of GWS changes occurred in December and was 0.80 ± 0.02 cm/year. In Ob, GWS increased slightly from February to May, ranging from 0.03 ± 0.01 to 0.11 ± 0.01 cm/year. GWS decreased in both Mackenzie and Yukon in all months. GWSA trends in Mackenzie were slight, ranging from −0.40 ± 0.01 to −0.07 ± 0.01 cm/year. GWSA trends in Yukon were significantly negative, ranging from −1.56 ± 0.02 to −1.12 ± 0.02 cm/year.

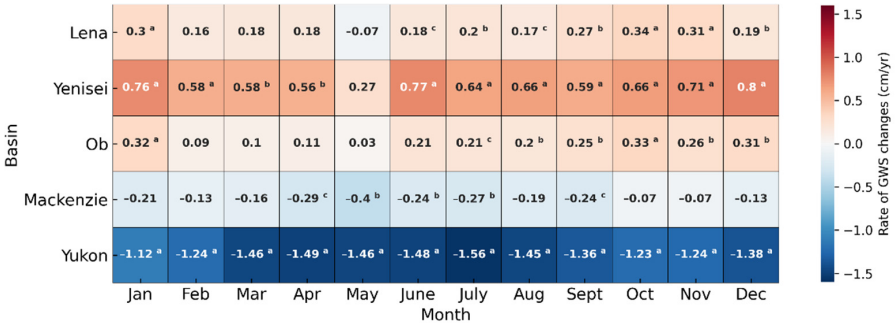



**Figure 4.** Trends in GWSA (cm/year) in different months over 2002–2017. The horizontal axis refers to months and vertical axis refers to the five basins. The value in each square of a panel refers to the rate of GWS change in a specific month over the 15-year period. The *p*-values were calculated using the Wald Test with a t-distribution of the test statistic. "[a]" refers to a *p*-value ≤ 0.01, "[b]" refers to 0.01 < *p*-value ≤ 0.05, and "[c]" refers to 0.05 < *p*-value ≤ 0.10.

### *4.3. Groundwater Storage Changes over 15 Years*

Figure 5 shows the GWSA time series, trends in GWSA, and annual rainfall anomalies in the five basins. Trends in GWSA were obtained using STL. GWSA trends were slightly positive in Lena in 2002–2017 (Figure 5a). GWS increased significantly from 2012 to 2014 in both Yenisei (Figure 5b) and Ob (Figure 5c). During this period, rainfall decreased. GWS also increased in Yenisei in 2015–2017, when rainfall increased significantly. GWSA trends were slightly negative in Mackenzie (Figure 5d). In Yukon, GWS decreased consistently from 2002 to 2016. Although the rainfall increased significantly from 2016 to 2017, GWS continued to decrease in Mackenzie and Yukon.

The rate of GWS changes in 2002–2017 in the five river basins are shown in Table 1. The rates of GWS changes were 0.20 ± 0.15 cm/year in Lena, 0.62 ± 0.12 cm/year in Yenisei and 0.20 ± 0.09 cm/year in Ob, which are equivalent to volume rates of 4.79 ± 3.75 $km^3$/year, 11.89 ± 2.29 $km^3$/year and 6.23 ± 2.81 $km^3$/year, respectively. GWS decreased at a rate of −0.21 ± 0.23 cm/year (−3.24 ± 3.48 $km^3$/year) in Mackenzie and −1.38 ± 0.23 cm/year (−11.51 ± 1.92 $km^3$/year) in Yukon in 2002–2017. GWS increased by up to 71.1 ± 55.6 $km^3$ in Lena, 176.3 ± 34.0 $km^3$ in Yenisei and 92.4 ± 41.7 $km^3$ in Ob in 2002–2017. In contrast, GWS decreased in Mackenzie and Yukon, by approximately 48.1 ± 51.7 $km^3$ and 170.7 ± 28.5 $km^3$, respectively.

**Table 1.** Rate of GWS changes and total GWS changes over 2002–2017 in the five pan-Arctic river basins *.

| Basin | Rate of GWS Changes | | Total GWS Changes over 15 Years |
|---|---|---|---|
| | cm/Year | $km^3$/Year | $km^3$/15 Years |
| Lena | 0.20 ± 0.15 | 4.79 ± 3.75 | 71.1 ± 55.6 |
| Yenisei | 0.62 ± 0.12 | 11.89 ± 2.29 | 176.3 ± 34.0 |
| Ob | 0.20 ± 0.09 | 6.23 ± 2.81 | 92.4 ± 41.7 |
| Mackenzie | −0.21 ± 0.23 | −3.24 ± 3.48 | −48.1 ± 51.7 |
| Yukon | −1.38 ± 0.23 | −11.51 ± 1.92 | −170.7 ± 28.5 |

* The *p*-values of the rates of GWS changes in the five basins are all <0.001.

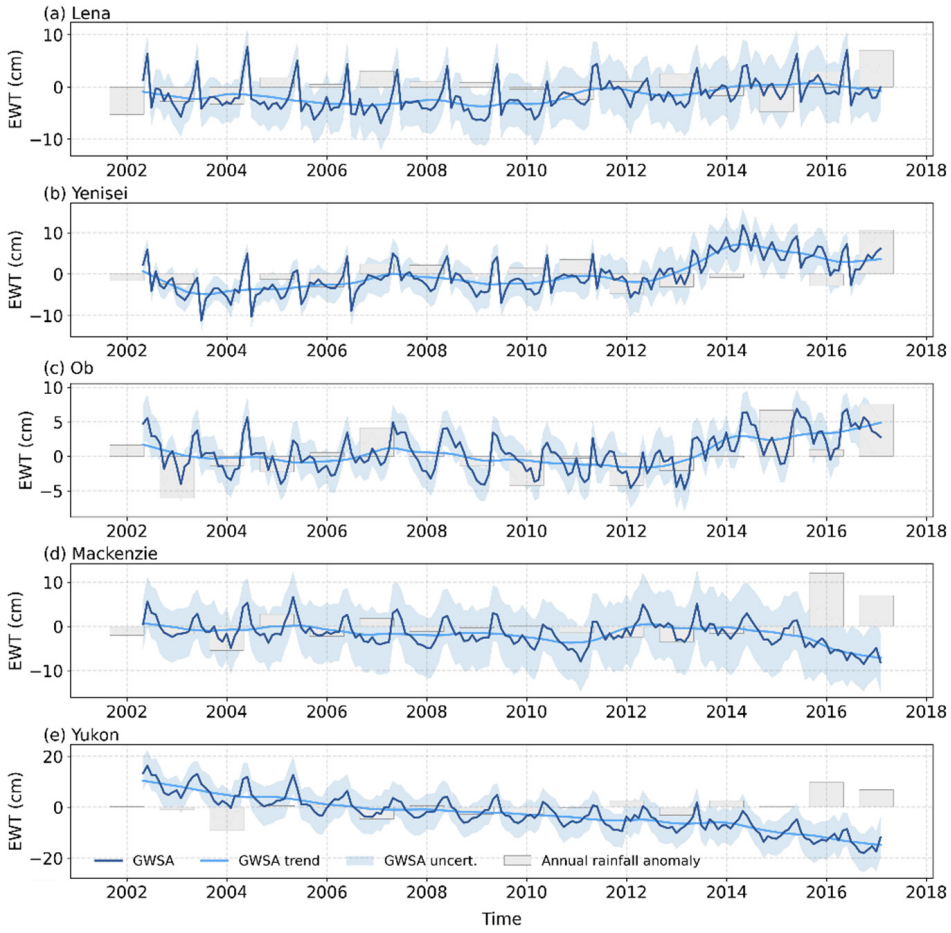



**Figure 5.** Monthly GWSA time series (deep blue line), trends in GWSA (light blue line), uncertainty in GWSA (light blue band), and annual rainfall anomaly (gray bar).

### *4.4. Surface Water Dynamics*

We categorized permanent, seasonal, ephemeral permanent, and ephemeral seasonal SW into unchanged SW types and categorized new permanent, new seasonal, lost permanent, lost seasonal, permanent to seasonal, and seasonal to permanent SW into changed SW types. Then, we calculated the area proportions of the six changed SW categories in each basin (Figure 6). New permanent and new seasonal SW were the primary contributors to SW dynamics in the past 35 years (1984–2019), accounting for more than 50% in each basin. There was an interesting pattern in Ob (Figure 6c): Much of the seasonal SW was lost (48.3%), while considerable new seasonal SW occurred (25.9%) during 1984–2019. In Mackenzie, lost permanent SW was one of the primary SW transition types compared with the other basins, with a proportion of 7.6%. Moreover, the transition between permanent and seasonal SW was also significant in Mackenzie, where the proportions of seasonal to permanent SW and permanent to seasonal SW were 15.1 and 13.7%, respectively.

Surface water dynamics for localized regions in the five basins are shown in Figure S2. Much new seasonal SW occurred in the localized regions of Lena, Yenisei, and Yukon. For the localized region in Mackenzie (Figure S2d), changes in lost permanent SW and permanent to seasonal SW were obvious. In Ob (Figure S2e), seasonal and permanent SW have undergone significant losses during the past 35 years.

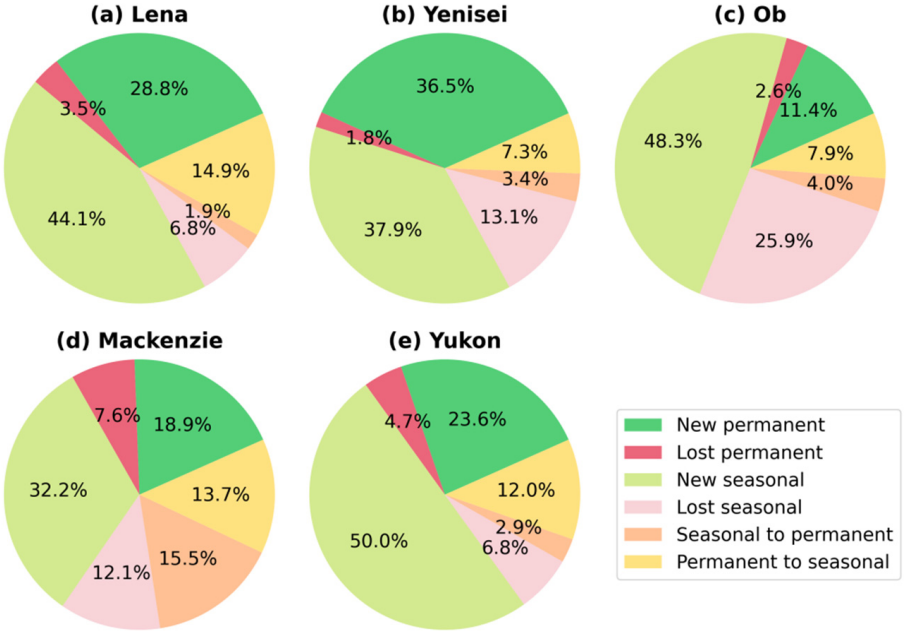



**Figure 6.** Area proportions of the six changed surface water categories in the five basins.

## 5. Discussion

We estimated GWS changes using remote sensing products, model products, and in situ measurements. The uncertainties in these input data mainly contributed to the uncertainties in GWS changes. Our results showed that the rates of GWS changes were $4.79 \pm 3.75$ km$^3$/year in Lena, $11.89 \pm 2.29$ km$^3$/year in Yenisei, $6.23 \pm 2.81$ km$^3$/year in Ob, $-3.24 \pm 3.48$ km$^3$/year in Mackenzie, and $-11.51 \pm 1.92$ km$^3$/year in Yukon from 2002 to 2017. In 2002–2008, the estimated rates of GWS changes were approximately 5.34 km$^3$/year in Lena, 23.11 km$^3$/year in Yenisei, 0.98 km$^3$/year in Ob, $-5.54$ km$^3$/year in Mackenzie, and $-7.44$ km$^3$/year in Yukon [61,62]. Our estimated rate in Ob was about six times higher than the result in 2002–2008. One of the main reasons is that GWS increased significantly in 2013–2017. Rainfall, SWE, and SM also increased during this period, which suggested that the climate in Ob was more humid. The rate in Yenisei in 2002–2017 was about one half of the rate in 2002–2008, though GWS increased significantly from 2012 to 2014. The rate in Yukon in 2002–2017 was about 1.5 times higher than the rate in 2002–2008. GWS in Yukon continued decreasing after 2008. During this period, changes in SWE and SM were slight. SM and SWE were not included when calculating GWS changes in 2002–2008 in the previous studies. This may also have contributed to the differences in the results despite the different study periods.

SM can be affected by active layer thickness and temperature through evaporation. A thicker active layer may decrease the water table in a basin and limit the terrestrial water available for evaporation [82]. A warming trend in soil temperature in permafrost regions was observed [83] and a higher temperature can enhance evaporation. Our results also showed that precipitation increased in the five basins during our study period, which may be related to climate change impact [64]. These results were consistent with the prediction of IPCC models that precipitation will generally increase in high latitudes [9]. Notably, the recent IPCC report highlighted the role of cooling aerosols (especially $SO_2$, nitrogen oxides, organic carbon, and ammonia) in countering part of the global warming [84]. Through radiation and interactions with clouds, these aerosols may influence the climate warming in the basins. Recent research revealed that the total emissions of $SO_2$ and nitrogen oxides in Eurasia were significantly less than those in North America [85]. This suggested that the cooling effect of the aerosols in Eurasia may be slighter than in North America and may further contribute to the differences in climate warming between the Siberian basins and North American basins. Moreover, geographical factors also contribute to differences in SM

and precipitation changes in the basins. The Yukon and Mackenzie Rivers are located in a significant part of the mountains. Mountains in Lena, Yenisei, and Ob occupy a relatively small share [34,86]. Generally, increasing annual precipitation has been observed in Arctic mountains, and this leads to increases in soil moisture and runoff [34].

A warming climate and permafrost thaw can increase subsurface hydrological connectivity [87]. The distribution and thickness of permafrost have significantly decreased in the Arctic over recent decades [88–90]. Permafrost thaw can increase GWS by increasing the infiltration rate of surface water into the ground [91] and accelerate the drainage of lakes [61]. On the other hand, permafrost thaw causes increasing groundwater discharge to streamflow, which can decrease groundwater storage [18,61]. A thickened active layer will accommodate more groundwater [34]. In the Siberian basins, the active layer thickness has generally increased during 1990–2006 because of thicker snowpacks and high summer soil moisture [92]. In the Mackenzie and Yukon basins, the warming effects on the active layer thickness have been partly offset owing to thinner snow depth and drier soil during summer in 1990–2006 [92]. This suggests that the impacts of the active layer on GWS changes during 2002–2006 in the Siberian basins are more significant than those in the Yukon and Mackenzie basins. In the Yukon basin, the existence of permafrost in subalpine zones in the mountains reduces GWS and enhances runoff [34].

Lake growth or shrinkage can be influenced by active layer dynamics and groundwater [93]. Initially, thickened active layers and melted ground ice cause the development of thermokarst lakes in Arctic lowlands where ice-rich and continuous permafrost is widespread [31,94]. The warming climate and the large heat capacity of lake water promote ground subsidence under the lake bottom and lake shore thawing, resulting in lake expansion [95,96]. Subsequently, permafrost degradation and thermoerosion cause lake drainage, leading to lake shrinkage and disappearance [31,97,98]. Decreased snow cover extent and snowmelt runoff can lead to shallow lakes drying by evaporation [99]. Warming temperature [31] and increased evapotranspiration [32] can lead to thinning and drainage of lakes. Wetting climate can lead to lake expansion [19,33]. In addition, geomorphologic factors, such as elevation, can influence lake area changes [33]. Increasing annual evapotranspiration has been observed in mountain regions and may cause drying [34]. Permafrost thaw and changes in streamflow affect river channels and river migration. The Siberian basins are mainly located in the temperate climatic zone, where the processes of permafrost degradation occur faster than in the North American basins. The effect of permafrost degradation on river runoff is more significant in the Siberian basins. Moreover, the distribution of permafrost affects river runoff dynamics. River runoff increased more significantly in the Lena, Yenisei, and Ob basins, where continuous permafrost occupied a larger share, than in the Yukon and Mackenzie basins [100]. These mechanisms mainly contributed to recent surface water body dynamics in pan-Arctic river basins.

Other factors also contributed to recent surface and groundwater dynamics. Snowfall is a substantial proportion of Arctic annual precipitation [101]. There was an increasing trend in SWE in the northern parts of the large Eurasian basins, despite a general decrease throughout the Arctic [101]. An increase in SWE can lead to increased annual runoff in these basins [102]. Generally, runoff increases during spring snowmelt and in summer. However, the seasonal flow for many Arctic rivers, including the Lena, Yenisei, and Mackenzie rivers, has been strongly influenced by dam construction [82,103]. Increased evapotranspiration has been observed in recent decades [4]. However, the Arctic annual evapotranspiration water flux is generally smaller than the annual precipitation [104]. Increases in evapotranspiration enhance the loss of water from river basins [105].

In this study, the uncertainty in GWS was mainly from the uncertainties in TWSA and SM and SWE. The accuracy of SWE was prominently affected by the presence of snow liquid water in the melt season. Liquid water increases the level of microwave emissivity. It also corrupts the sensitivity of the observed brightness temperature to changes in SWE because increasing moisture decreases the penetration depth of microwave radiation in snowpacks [77]. The SW and GWS changes were not from the same period because of

the different periods of the SW transition and TWS products. This created uncertainty in the joint analysis of surface and groundwater dynamics. However, these two products individually provided the latest results with the longest time span. We aimed to use the products with the longest time span to evaluate the changes during the period in which satellite observations were available. GRACE data helped to evaluate GWS changes at large scales and provided scientific support for future water resource assessments. More accurate models for the Arctic permafrost region are required to provide more accurate SM data, which can improve the quality of the estimated results.

## 6. Conclusions

In this study, GWS changes in the five large pan-Arctic river basins during 2002–2017 were obtained based on GRACE-derived TWSA, SWE from remote sensing products, soil moisture from models, and in situ runoff. Surface water changes in the basins during 1984–2019 were obtained based on the JRC surface water transition product. We found that over the past 15 years (2002–2017), GWS increased in the Siberian river basins, totaling ~340 $km^3$, and decreased in the North American basins, totaling approximately −219 $km^3$. We also found that new permanent and new seasonal surface water bodies were the primary contributors to surface water dynamics, accounting for more than 50% in each basin in 1984–2019. In the future, continued and intensified climate warming and permafrost thaw will lead to more significant and various changes in Arctic surface and groundwater.

This study focused on providing a new evaluation of groundwater and surface water dynamics in large pan-Arctic river basins in recent decades. It remains challenging to profoundly analyze the specific drivers of surface and groundwater changes. This study highlighted the value of the remote sensing technique in evaluating groundwater and surface water changes at large spatial scales. The groundwater and surface water changes in the five basins during the longest satellite period are presented in the study. This study provides scientific support for future water resource assessments. Furthermore, it helps us to better understand the Arctic hydrological fluxes and storage at a large watershed scale and the connection between permafrost hydrology and climate, which are critical for the Arctic water balance, environment, ecology, and economy.

**Supplementary Materials:** The following supporting information can be downloaded at: https://www.mdpi.com/article/10.3390/rs14030607/s1, Figure S1: Monthly TWSA (deep blue line), SMSA (red dashed line), SnWSA (light blue dashed line) and RA (gray bar) time series from April 2002 to January 2017 in Lena, Yenisei, Ob, Mackenzie and Yukon. EWT refers to equivalent water thickness; Figure S2: Surface water changes for localized regions in the five basins during 1984–2019 (data source: EC JRC/Google, accessed on 31 March 2021) (Pekel et al., 2016). Map in a, b, c, d and e shows the surface water transition in the localized regions in Lena, Yenisei, Ob, Mackenzie and Yukon, respectively.

**Author Contributions:** Conceptualization, L.Z. and W.F.; methodology, L.Z., W.F. and F.P.; software, H.L.; validation, H.L.; formal analysis, L.Z. and H.L.; investigation, L.Z., X.P. and H.L.; resources, X.C.; data curation, H.L.; writing—original draft preparation, H.L.; writing—review and editing, X.C., L.Z., X.P. and F.P.; visualization, H.L.; supervision, X.C.; project administration, X.C.; funding acquisition, X.C. All authors have read and agreed to the published version of the manuscript.

**Funding:** This research was funded by the National Key Research and Development Program of China (Grant No. 2019YFC1509104) and the Innovation Group Project of Southern Marine Science and Engineering Guangdong Laboratory (Zhuhai) (No. 311021008).

**Institutional Review Board Statement:** Not applicable.

**Informed Consent Statement:** Not applicable.

**Data Availability Statement:** Not applicable.

**Acknowledgments:** We thank the reviewers for their suggestions, which improved the quality of this paper, and thank Mi Jiang for his helpful suggestions.

**Conflicts of Interest:** The authors declare no conflict of interest.

## References


1. Fichot, C.G.; Kaiser, K.; Hooker, S.B.; Amon, R.M.W.; Babin, M.; Bélanger, S.; Walker, S.A.; Benner, R. Pan-Arctic distributions of continental runoff in the Arctic Ocean. *Sci. Rep.* **2013**, *3*, 1053. [CrossRef] [PubMed]
2. Lique, C.; Holland, M.M.; Dibike, Y.B.; Lawrence, D.M.; Screen, J.A. Modeling the Arctic freshwater system and its integration in the global system: Lessons learned and future challenges. *J. Geophys. Res. G Biogeosci.* **2016**, *121*, 540–566. [CrossRef]
3. Morison, J.; Kwok, R.; Peralta-Ferriz, C.; Alkire, M.; Rigor, I.; Andersen, R.; Steele, M. Changing Arctic Ocean freshwater pathways. *Nature* **2012**, *481*, 66–70. [CrossRef] [PubMed]
4. Rawlins, M.A.; Steele, M.; Holland, M.M.; Adam, J.C.; Cherry, J.E.; Francis, J.A.; Groisman, P.Y.; Hinzman, L.D.; Huntington, T.G.; Kane, D.L.; et al. Analysis of the Arctic system for freshwater cycle intensification: Observations and expectations. *J. Clim.* **2010**, *23*, 5715–5737. [CrossRef]
5. Rowland, J.C.; Jones, C.E.; Altmann, G.; Bryan, R.; Crosby, B.T.; Geernaert, G.L.; Hinzman, L.D.; Kane, D.L.; Lawrence, D.M.; Mancino, A.; et al. Arctic landscapes in transition: Responses to thawing permafrost. *Eos* **2010**, *91*, 229–230. [CrossRef]
6. Cohen, J.; Screen, J.A.; Furtado, J.C.; Barlow, M.; Whittleston, D.; Coumou, D.; Francis, J.; Dethloff, K.; Entekhabi, D.; Overland, J.; et al. Recent Arctic amplification and extreme mid-latitude weather. *Nat. Geosci.* **2014**, *7*, 627–637. [CrossRef]
7. Polyakov, I.V.; Alekseev, G.V.; Bekryaev, R.V.; Bhatt, U.; Colony, R.L.; Johnson, M.A.; Karklin, V.P.; Makshtas, A.P.; Walsh, D.; Yulin, A.V. Observationally based assessment of polar amplification of global warming. *Geophys. Res. Lett.* **2002**, *29*, 1878. [CrossRef]
8. Serreze, M.C.; Stroeve, J. Arctic sea ice trends, variability and implications for seasonal ice forecasting. *Philos. Trans. R. Soc. A Math. Phys. Eng. Sci.* **2015**, *373*, 20140159. [CrossRef] [PubMed]
9. Stocker, T. *Climate Change 2013: The Physical Science Basis: Working Group I Contribution to the Fifth Assessment Report of the Intergovernmental Panel on Climate Change*; Cambridge University Press: Cambridge, UK, 2014; ISBN 110705799X.
10. Zhang, T. Influence of the seasonal snow cover on the ground thermal regime: An overview. *Rev. Geophys.* **2005**, *43*, RG4002. [CrossRef]
11. Woo, M.K.; Kane, D.L.; Carey, S.K.; Yang, D. Progress in permafrost hydrology in the new millennium. *Permafr. Periglac. Process.* **2008**, *19*, 237–254. [CrossRef]
12. Shugar, D.H.; Jacquemart, M.; Shean, D.; Bhushan, S.; Upadhyay, K.; Sattar, A.; Schwanghart, W.; McBride, S.; de Vries, M.V.W.; Mergili, M. A massive rock and ice avalanche caused the 2021 disaster at Chamoli, Indian Himalaya. *Science* **2021**, *373*, 300–306. [CrossRef]
13. Zhang, T.; Barry, R.G.; Knowles, K.; Heginbottom, J.A.; Brown, J. Statistics and characteristics of permafrost and ground-ice distribution in the Northern Hemisphere. *Polar Geogr.* **1999**, *23*, 132–154. [CrossRef]
14. Brown, J.; Ferrians, O.J., Jr.; Heginbottom, J.A.; Melnikov, E.S. *Circum-Arctic Map of Permafrost and Ground Ice Conditions*; US Geological Survey Reston: Reston, VA, USA, 1997; ISBN 0607887451.
15. Zhang, T.; Frauenfeld, O.W.; Serreze, M.C.; Etringer, A.; Oelke, C.; McCreight, J.; Barry, R.G.; Gilichinsky, D.; Yang, D.; Ye, H.; et al. Spatial and temporal variability in active layer thickness over the Russian Arctic drainage basin. *J. Geophys. Res. D Atmos.* **2005**, *110*, D16101. [CrossRef]
16. Liljedahl, A.K.; Boike, J.; Daanen, R.P.; Fedorov, A.N.; Frost, G.V.; Grosse, G.; Hinzman, L.D.; Iijma, Y.; Jorgenson, J.C.; Matveyeva, N. Pan-Arctic ice-wedge degradation in warming permafrost and its influence on tundra hydrology. *Nat. Geosci.* **2016**, *9*, 312–318. [CrossRef]
17. Walvoord, M.A.; Voss, C.I.; Wellman, T.P. Influence of permafrost distribution on groundwater flow in the context of climate-driven permafrost thaw: Example from Yukon Flats Basin, Alaska, United States. *Water Resour. Res.* **2012**, *48*, W07524. [CrossRef]
18. Ge, S.; McKenzie, J.; Voss, C.; Wu, Q. Exchange of groundwater and surface-water mediated by permafrost response to seasonal and long term air temperature variation. *Geophys. Res. Lett.* **2011**, *38*, L14402. [CrossRef]
19. Monitoring, A. *Snow, Water, Ice and Permafrost in the Arctic (SWIPA) 2017*; Arctic Council Secretariat: Tromsø, Norway, 2017.
20. Brown, J.; Ferrians, O.; Heginbottom, J.A.; Melnikov, E. *Circum-Arctic Map of Permafrost and Ground-Ice Conditions, Version 2*; NSIDC: National Snow and Ice Data Center: Boulder, CO, USA, 2002.
21. McClelland, J.W.; Déry, S.J.; Peterson, B.J.; Holmes, R.M.; Wood, E.F. A pan-arctic evaluation of changes in river discharge during the latter half of the 20th century. *Geophys. Res. Lett.* **2006**, *33*, L06715. [CrossRef]
22. Overeem, I.; Syvitski, J.P.M. Shifting discharge peaks in arctic rivers, 1977–2007. *Geogr. Ann. Ser. A Phys. Geogr.* **2010**, *92*, 285–296. [CrossRef]
23. Peterson, B.J.; Holmes, R.M.; McClelland, J.W.; Vörösmarty, C.J.; Lammers, R.B.; Shiklomanov, A.I.; Shiklomanov, I.A.; Rahmstorf, S. Increasing river discharge to the Arctic Ocean. *Science* **2002**, *298*, 2171–2173. [CrossRef]
24. Rood, S.B.; Kaluthota, S.; Philipsen, L.J.; Rood, N.J.; Zanewich, K.P. Increasing discharge from the Mackenzie River system to the Arctic Ocean. *Hydrol. Process.* **2017**, *31*, 150–160. [CrossRef]
25. Wang, P.; Huang, Q.; Pozdniakov, S.P.; Liu, S.; Ma, N.; Wang, T.; Zhang, Y.; Yu, J.; Xie, J.; Fu, G.; et al. Potential role of permafrost thaw on increasing Siberian river discharge. *Environ. Res. Lett.* **2021**, *16*, 034046. [CrossRef]
26. Zhang, X.; Tang, Q.; Liu, X.; Leng, G.; Di, C. Nonlinearity of Runoff Response to Global Mean Temperature Change Over Major Global River Basins. *Geophys. Res. Lett.* **2018**, *45*, 6109–6116. [CrossRef]

27. Ling, F.; Zhang, T. Modeling study of talik freeze-up and permafrost response under drained thaw lakes on the Alaskan Arctic Coastal Plain. *J. Geophys. Res. Atmos.* **2004**, *109*, D01111. [CrossRef]
28. Zheng, L.; Overeem, I.; Wang, K.; Clow, G.D. Changing Arctic River Dynamics Cause Localized Permafrost Thaw. *J. Geophys. Res. Earth Surf.* **2019**, *124*, 2324–2344. [CrossRef]
29. Osterkamp, T.E.; Gosink, J.P. Variations in permafrost thickness in response to changes in paleoclimate. *J. Geophys. Res.* **1991**, *96*, 4423–4434. [CrossRef]
30. Walvoord, M.A.; Kurylyk, B.L. Hydrologic Impacts of Thawing Permafrost—A Review. *Vadose Zone J.* **2016**, *15*, 6. [CrossRef]
31. Smith, L.C.; Sheng, Y.; MacDonald, G.M.; Hinzman, L.D. Atmospheric Science: Disappearing Arctic lakes. *Science* **2005**, *308*, 1429. [CrossRef]
32. Andresen, C.G.; Lougheed, V.L. Disappearing Arctic tundra ponds: Fine-scale analysis of surface hydrology in drained thaw lake basins over a 65 year period (1948-2013). *J. Geophys. Res. Biogeosci.* **2015**, *120*, 466–479. [CrossRef]
33. Veremeeva, A.; Nitze, I.; Günther, F.; Grosse, G.; Rivkina, E. Geomorphological and climatic drivers of thermokarst lake area increase trend (1999–2018) in the kolyma lowland yedoma region, north-eastern siberia. *Remote Sens.* **2021**, *13*, 178. [CrossRef]
34. Bring, A.; Fedorova, I.; Dibike, Y.; Hinzman, L.; Mård, J.; Mernild, S.H.; Prowse, T.; Semenova, O.; Stuefer, S.L.; Woo, M.K. Arctic terrestrial hydrology: A synthesis of processes, regional effects, and research challenges. *J. Geophys. Res. G Biogeosci.* **2016**, *121*, 621–649. [CrossRef]
35. Green, T.R.; Taniguchi, M.; Kooi, H.; Gurdak, J.J.; Allen, D.M.; Hiscock, K.M.; Treidel, H.; Aureli, A. Beneath the surface of global change: Impacts of climate change on groundwater. *J. Hydrol.* **2011**, *405*, 532–560. [CrossRef]
36. Lecher, A.L. Groundwater discharge in the Arctic: A review of studies and implications for biogeochemistry. *Hydrology* **2017**, *4*, 41. [CrossRef]
37. Bense, V.F.; Kooi, H.; Ferguson, G.; Read, T. Permafrost degradation as a control on hydrogeological regime shifts in a warming climate. *J. Geophys. Res. Earth Surf.* **2012**, *117*, F03036. [CrossRef]
38. Kane, D.L.; Yoshikawa, K.; McNamara, J.P. Regional groundwater flow in an area mapped as continuous permafrost, NE Alaska (USA). *Hydrogeol. J.* **2013**, *21*, 41–52. [CrossRef]
39. Connolly, C.T.; Cardenas, M.B.; Burkart, G.A.; Spencer, R.G.M.; McClelland, J.W. Groundwater as a major source of dissolved organic matter to Arctic coastal waters. *Nat. Commun.* **2020**, *11*, 1479. [CrossRef]
40. Black, F.J.; Paytan, A.; Knee, K.L.; De Sieyes, N.R.; Ganguli, P.M.; Gray, E.; Flegal, A.R. Submarine groundwater discharge of total mercury and monomethylmercury to central California coastal waters. *Environ. Sci. Technol.* **2009**, *43*, 5652–5659. [CrossRef]
41. Knee, K.L.; Gossett, R.; Boehm, A.B.; Paytan, A. Caffeine and agricultural pesticide concentrations in surface water and groundwater on the north shore of Kauai (Hawaii, USA). *Mar. Pollut. Bull.* **2010**, *60*, 1376–1382. [CrossRef]
42. Knee, K.L.; Layton, B.A.; Street, J.H.; Boehm, A.B.; Paytan, A. Sources of nutrients and fecal indicator bacteria to nearshore waters on the north shore of Kauai (Hawaii, USA). *Estuaries Coasts* **2008**, *31*, 607–622. [CrossRef]
43. Lecher, A.L.; Kessler, J.; Sparrow, K.; Garcia-Tigreros Kodovska, F.; Dimova, N.; Murray, J.; Tulaczyk, S.; Paytan, A. Methane transport through submarine groundwater discharge to the North Pacific and Arctic Ocean at two Alaskan sites. *Limnol. Oceanogr.* **2016**, *61*, S344–S355. [CrossRef]
44. Paytan, A.; Lecher, A.L.; Dimova, N.; Sparrow, K.J.; Garcia-Tigreros Kodovska, F.; Murray, J.; Tulaczyk, S.; Kessler, J.D. Methane transport from the active layer to lakes in the Arctic using Toolik Lake, Alaska, as a case study. *Proc. Natl. Acad. Sci. USA* **2015**, *112*, 3636–3640. [CrossRef]
45. Walvoord, M.A.; Striegl, R.G. Increased groundwater to stream discharge from permafrost thawing in the Yukon River basin: Potential impacts on lateral export of carbon and nitrogen. *Geophys. Res. Lett.* **2007**, *34*, L12402. [CrossRef]
46. Dimova, N.T.; Paytan, A.; Kessler, J.D.; Sparrow, K.J.; Garcia-Tigreros Kodovska, F.; Lecher, A.L.; Murray, J.; Tulaczyk, S.M. Current Magnitude and Mechanisms of Groundwater Discharge in the Arctic: Case Study from Alaska. *Environ. Sci. Technol.* **2015**, *49*, 12036–12043. [CrossRef] [PubMed]
47. Verpoorter, C.; Kutser, T.; Seekell, D.A.; Tranvik, L.J. A global inventory of lakes based on high-resolution satellite imagery. *Geophys. Res. Lett.* **2014**, *41*, 6396–6402. [CrossRef]
48. Feng, M.; Sexton, J.O.; Channan, S.; Townshend, J.R. A global, high-resolution (30-m) inland water body dataset for 2000: First results of a topographic–spectral classification algorithm. *Int. J. Digit. Earth* **2016**, *9*, 113–133. [CrossRef]
49. Yamazaki, D.; Trigg, M.A.; Ikeshima, D. Development of a global ~90 m water body map using multi-temporal Landsat images. *Remote Sens. Environ.* **2015**, *171*, 337–351. [CrossRef]
50. Prigent, C.; Papa, F.; Aires, F.; Jimenez, C.; Rossow, W.B.; Matthews, E. Changes in land surface water dynamics since the 1990s and relation to population pressure. *Geophys. Res. Lett.* **2012**, *39*, L08403. [CrossRef]
51. Pekel, J.F.; Cottam, A.; Gorelick, N.; Belward, A.S. High-resolution mapping of global surface water and its long-term changes. *Nature* **2016**, *540*, 418–422. [CrossRef]
52. Park, S.-E. Variations of microwave scattering properties by seasonal freeze/thaw transition in the permafrost active layer observed by ALOS PALSAR polarimetric data. *Remote Sens.* **2015**, *7*, 17135–17148. [CrossRef]
53. Gascoin, S.; Grizonnet, M.; Bouchet, M.; Salgues, G.; Hagolle, O. Theia Snow collection: High-resolution operational snow cover maps from Sentinel-2 and Landsat-8 data. *Earth Syst. Sci. Data* **2019**, *11*, 493–514. [CrossRef]

54. Muhuri, A.; Gascoin, S.; Menzel, L.; Kostadinov, T.S.; Harpold, A.A.; Sanmiguel-Vallelado, A.; López-Moreno, J.I. Performance Assessment of Optical Satellite-Based Operational Snow Cover Monitoring Algorithms in Forested Landscapes. *IEEE J. Sel. Top. Appl. Earth Obs. Remote Sens.* **2021**, *14*, 7159–7178. [CrossRef]
55. Feng, W.; Zhong, M.; Lemoine, J.M.; Biancale, R.; Hsu, H.T.; Xia, J. Evaluation of groundwater depletion in North China using the Gravity Recovery and Climate Experiment (GRACE) data and ground-based measurements. *Water Resour. Res.* **2013**, *49*, 2110–2118. [CrossRef]
56. Rodell, M.; Velicogna, I.; Famiglietti, J.S. Satellite-based estimates of groundwater depletion in India. *Nature* **2009**, *460*, 999–1002. [CrossRef] [PubMed]
57. Longuevergne, L.; Scanlon, B.R.; Wilson, C.R. GRACE Hydrological estimates for small basins: Evaluating processing approaches on the High Plains Aquifer, USA. *Water Resour. Res.* **2010**, *46*, W11517. [CrossRef]
58. Famiglietti, J.S.; Lo, M.; Ho, S.L.; Bethune, J.; Anderson, K.J.; Syed, T.H.; Swenson, S.C.; de Linage, C.R.; Rodell, M. Satellites measure recent rates of groundwater depletion in California's Central Valley. *Geophys. Res. Lett.* **2011**, *38*, L03403. [CrossRef]
59. Voss, K.A.; Famiglietti, J.S.; Lo, M.; De Linage, C.; Rodell, M.; Swenson, S.C. Groundwater depletion in the Middle East from GRACE with implications for transboundary water management in the Tigris-Euphrates-Western Iran region. *Water Resour. Res.* **2013**, *49*, 904–914. [CrossRef] [PubMed]
60. Rateb, A.; Scanlon, B.R.; Pool, D.R.; Sun, A.; Zhang, Z.; Chen, J.; Clark, B.; Faunt, C.C.; Haugh, C.J.; Hill, M.; et al. Comparison of Groundwater Storage Changes From GRACE Satellites With Monitoring and Modeling of Major U.S. Aquifers. *Water Resour. Res.* **2020**, *56*, e2020WR027556. [CrossRef]
61. Muskett, R.R.; Romanovsky, V.E. Alaskan Permafrost groundwater storage changes derived from GRACE and ground measurements. *Remote Sens.* **2011**, *3*, 378. [CrossRef]
62. Muskett, R.R.; Romanovsky, V.E. Groundwater storage changes in arctic permafrost watersheds from GRACE and insitu measurements. *Environ. Res. Lett.* **2009**, *4*, 045009. [CrossRef]
63. Tapley, B.D.; Watkins, M.M.; Flechtner, F.; Reigber, C.; Bettadpur, S.; Rodell, M.; Sasgen, I.; Famiglietti, J.S.; Landerer, F.W.; Chambers, D.P.; et al. Contributions of GRACE to understanding climate change. *Nat. Clim. Chang.* **2019**, *9*, 358–369. [CrossRef]
64. Rodell, M.; Famiglietti, J.S.; Wiese, D.N.; Reager, J.T.; Beaudoing, H.K.; Landerer, F.W.; Lo, M.H. Emerging trends in global freshwater availability. *Nature* **2018**, *557*, 651–659. [CrossRef]
65. Richey, A.S.; Thomas, B.F.; Lo, M.; Famiglietti, J.S.; Swenson, S.; Rodell, M. Uncertainty in global groundwater storage estimates in a T otal G roundwater S tress framework. *Water Resour. Res.* **2015**, *51*, 5198–5216. [CrossRef] [PubMed]
66. Döll, P.; Mueller Schmied, H.; Schuh, C.; Portmann, F.T.; Eicker, A. Global-scale assessment of groundwater depletion and related groundwater abstractions: Combining hydrological modeling with information from well observations and GRACE satellites. *Water Resour. Res.* **2014**, *50*, 5698–5720. [CrossRef]
67. Famiglietti, J.S. The global groundwater crisis. *Nat. Clim. Chang.* **2014**, *4*, 945–948. [CrossRef]
68. Cleveland, R.B.; Cleveland, W.S.; McRae, J.E.; Terpenning, I. STL: A Seasonal-Trend Decomposition Procedure Based on Loess. *J. Off. Stat.* **1990**, *6*, 3–73.
69. Landerer, F.W.; Swenson, S.C. Accuracy of scaled GRACE terrestrial water storage estimates. *Water Resour. Res.* **2012**, *48*, W04531. [CrossRef]
70. Swenson, S.; Wahr, J. Post-processing removal of correlated errors in GRACE data. *Geophys. Res. Lett.* **2006**, *33*, L08402. [CrossRef]
71. Swenson, S.C. *Grace Monthly Land Water Mass Grids Netcdf Release 5.0., Ver. 5.0.*; PO.DAAC: Pasadena, CA, USA, 2012.
72. Rodell, M.; Houser, P.R.; Jambor, U.E.A.; Gottschalck, J.; Mitchell, K.; Meng, C.-J.; Arsenault, K.; Cosgrove, B.; Radakovich, J.; Bosilovich, M. The global land data assimilation system. *Bull. Am. Meteorol. Soc.* **2004**, *85*, 381–394. [CrossRef]
73. McNally, A. *FLDAS Noah Land Surface Model L4 Global Monthly 0.1 × 0.1 Degree (MERRA-2 and CHIRPS)*; Goddard Earth Sciences Data and Information Services Center: Greenbelt, MD, USA, 2018. [CrossRef]
74. Luojus, K.; Pulliainen, J.; Takala, M.; Lemmetyinen, J.; Moisander, M. *GlobSnow v3.0 Snow Water Equivalent (SWE)*; PANGAEA: Bremen, Germany, 2020.
75. Lemmetyinen, J.; Pulliainen, J.; Rees, A.; Kontu, A.; Qiu, Y.; Derksen, C. Multiple-layer adaptation of HUT snow emission model: Comparison with experimental data. *IEEE Trans. Geosci. Remote Sens.* **2010**, *48*, 2781–2794. [CrossRef]
76. Pulliainen, J.T.; Grandeil, J.; Hallikainen, M.T. HUT snow emission model and its applicability to snow water equivalent retrieval. *IEEE Trans. Geosci. Remote Sens.* **1999**, *37*, 1378–1390. [CrossRef]
77. Pulliainen, J. Mapping of snow water equivalent and snow depth in boreal and sub-arctic zones by assimilating space-borne microwave radiometer data and ground-based observations. *Remote Sens. Environ.* **2006**, *101*, 257–269. [CrossRef]
78. Takala, M.; Luojus, K.; Pulliainen, J.; Derksen, C.; Lemmetyinen, J.; Kärnä, J.P.; Koskinen, J.; Bojkov, B. Estimating northern hemisphere snow water equivalent for climate research through assimilation of space-borne radiometer data and ground-based measurements. *Remote Sens. Environ.* **2011**, *115*, 3517–3529. [CrossRef]
79. Pulliainen, J.; Luojus, K.; Derksen, C.; Mudryk, L.; Lemmetyinen, J.; Salminen, M.; Ikonen, J.; Takala, M.; Cohen, J.; Smolander, T.; et al. Patterns and trends of Northern Hemisphere snow mass from 1980 to 2018. *Nature* **2020**, *581*, 294–298. [CrossRef] [PubMed]
80. Shiklomanov, A.I.; Holmes, R.M.; McClelland, J.W.; Tank, S.E.; Spencer, R.G.M. Arctic Great Rivers Observatory. Discharge Dataset, Version 20180527. Technical Report. 2021. Available online: https://arcticgreatrivers.org/discharge/ (accessed on 13 December 2021).

81. Bevington, P.R.; Robinson, D.K.; Blair, J.M.; Mallinckrodt, A.J.; McKay, S. Data reduction and error analysis for the physical sciences. *Comput. Phys.* **1993**, *7*, 415–416. [CrossRef]
82. McClelland, J.W.; Holmes, R.M.; Peterson, B.J.; Stieglitz, M. Increasing river discharge in the Eurasian Arctic: Consideration of dams, permafrost thaw, and fires as potential agents of change. *J. Geophys. Res. Atmos.* **2004**, *109*, D18102. [CrossRef]
83. Romanovsky, V.E.; Sazonova, T.S.; Balobaev, V.T.; Shender, N.I.; Sergueev, D.O. Past and recent changes in air and permafrost temperatures in eastern Siberia. *Glob. Planet. Change* **2007**, *56*, 399–413. [CrossRef]
84. IPCC. Summary for Policymakers. In *Climate Change 2021: The Physical Science Basis Contribution of Working Group I to the Sixth Assessment Report of the Intergovernmental Panel on Climate Change*; IPCC: Geneva, Switzerland, 2021; ISBN 9789291691586.
85. Ye, Q.; Li, J.; Chen, X.; Chen, H.; Yang, W.; Du, H.; Pan, X.; Tang, X.; Wang, W.; Zhu, L. High-resolution modeling of the distribution of surface air pollutants and their intercontinental transport by a global tropospheric atmospheric chemistry source–receptor model (GNAQPMS-SM). *Geosci. Model Dev.* **2021**, *14*, 7573–7604. [CrossRef]
86. Adam, J.C.; Clark, E.A.; Lettenmaier, D.P.; Wood, E.F. Correction of global precipitation products for orographic effects. *J. Clim.* **2006**, *19*, 15–38. [CrossRef]
87. Song, C.; Wang, G.; Sun, X.; Hu, Z. River runoff components change variably and respond differently to climate change in the Eurasian Arctic and Qinghai-Tibet Plateau permafrost regions. *J. Hydrol.* **2021**, *601*, 126653. [CrossRef]
88. Walsh, J.; Anisimov, O.; Hagen, J.O.; Jakobsson, T.; Oerlemans, J.; Prowse, T.D.; Romanovsky, V.; Savelieva, N.; Serreze, M.; Shiklomanov, A. *Cryosphere and Hydrology Arctic Climate Impact Assessment*; ACIA Secretariat and Cooperative Institute for Arctic Research: Cambridge, UK, 2005; pp. 183–242.
89. Romanovsky, V.E.; Smith, S.L.; Christiansen, H.H. Permafrost thermal state in the polar Northern Hemisphere during the international polar year 2007–2009: A synthesis. *Permafr. Periglac. Process.* **2010**, *21*, 106–116. [CrossRef]
90. Jin, H.J.; Wu, Q.B.; Romanovsky, V.E. Degrading permafrost and its impacts. *Adv. Clim. Chang. Res.* **2021**, *12*, 1–5. [CrossRef]
91. Kurylyk, B.L.; Watanabe, K. The mathematical representation of freezing and thawing processes in variably-saturated, non-deformable soils. *Adv. Water Resour.* **2013**, *60*, 160–177. [CrossRef]
92. Park, H.; Walsh, J.; Fedorov, A.N.; Sherstiukov, A.B.; Iijima, Y.; Ohata, T. The influence of climate and hydrological variables on opposite anomaly in active-layer thickness between Eurasian and North American watersheds. *Cryosphere* **2013**, *7*, 631–645. [CrossRef]
93. Jepsen, S.M.; Voss, C.I.; Walvoord, M.A.; Minsley, B.J.; Rover, J. Linkages between lake shrinkage/expansion and sublacustrine permafrost distribution determined from remote sensing of interior Alaska, USA. *Geophys. Res. Lett.* **2013**, *40*, 882–887. [CrossRef]
94. Muster, S.; Roth, K.; Langer, M.; Lange, S.; Cresto Aleina, F.; Bartsch, A.; Morgenstern, A.; Grosse, G.; Jones, B.; Sannel, A.B.K. PeRL: A circum-Arctic permafrost region pond and lake database. *Earth Syst. Sci. Data* **2017**, *9*, 317–348. [CrossRef]
95. Hinkel, K.M.; Sheng, Y.; Lenters, J.D.; Lyons, E.A.; Beck, R.A.; Eisner, W.R.; Wang, J. Thermokarst Lakes on the Arctic Coastal Plain of Alaska: Geomorphic Controls on Bathymetry. *Permafr. Periglac. Process.* **2012**, *23*, 218–230. [CrossRef]
96. Jones, B.M.; Grosse, G.; Arp, C.D.; Jones, M.C.; Walter Anthony, K.M.; Romanovsky, V.E. Modern thermokarst lake dynamics in the continuous permafrost zone, northern Seward Peninsula, Alaska. *J. Geophys. Res. Biogeosci.* **2011**, *116*, G00M03. [CrossRef]
97. Günther, F.; Overduin, P.P.; Yakshina, I.A.; Opel, T.; Baranskaya, A.V.; Grigoriev, M.N. Observing Muostakh disappear: Permafrost thaw subsidence and erosion of a ground-ice-rich Island in response to arctic summer warming and sea ice reduction. *Cryosphere* **2015**, *9*, 151–178. [CrossRef]
98. Yoshikawa, K.; Hinzman, L.D. Shrinking thermokarst ponds and groundwater dynamics in discontinuous permafrost near Council, Alaska. *Permafr. Periglac. Process.* **2003**, *14*, 151–160. [CrossRef]
99. Bouchard, F.; Turner, K.W.; MacDonald, L.A.; Deakin, C.; White, H.; Farquharson, N.; Medeiros, A.S.; Wolfe, B.B.; Hall, R.I.; Pienitz, R. Vulnerability of shallow subarctic lakes to evaporate and desiccate when snowmelt runoff is low. *Geophys. Res. Lett.* **2013**, *40*, 6112–6117. [CrossRef]
100. Feng, D.; Gleason, C.J.; Lin, P.; Yang, X.; Pan, M.; Ishitsuka, Y. Recent changes to Arctic river discharge. *Nat. Commun.* **2021**, *12*, 6917. [CrossRef]
101. Liston, G.E.; Hiemstra, C.A. The changing cryosphere: Pan-Arctic snow trends (1979–2009). *J. Clim.* **2011**, *24*, 5691–5712. [CrossRef]
102. Troy, T.J.; Sheffield, J.; Wood, E.F. The role of winter precipitation and temperature on northern Eurasian streamflow trends. *J. Geophys. Res. Atmos.* **2012**, *117*, D05131. [CrossRef]
103. Yang, D.; Shi, X.; Marsh, P. Variability and extreme of Mackenzie River daily discharge during 1973–2011. *Quat. Int.* **2015**, *380*, 159–168. [CrossRef]
104. Serreze, M.C.; Barrett, A.P.; Slater, A.G.; Woodgate, R.A.; Aagaard, K.; Lammers, R.B.; Steele, M.; Moritz, R.; Meredith, M.; Lee, C.M. The large-scale freshwater cycle of the Arctic. *J. Geophys. Res. Ocean.* **2006**, *111*, C11010. [CrossRef]
105. Wrona, F.J.; Johansson, M.; Culp, J.M.; Jenkins, A.; Mård, J.; Myers-Smith, I.H.; Prowse, T.D.; Vincent, W.F.; Wookey, P.A. Transitions in Arctic ecosystems: Ecological implications of a changing hydrological regime. *J. Geophys. Res. Biogeosci.* **2016**, *121*, 650–674. [CrossRef]